ISBN: 978-3-95450-214-1 ISSN: 2673-5490 doi:10.18429/JACoW-IPAC2021-WEPAB025

COLLIMATION STRATEGIES FOR SECONDARY BEAMS IN FCC-hh ION-ION OPERATION

J. R. Hunt*, R. Bruce, F. Carra. F. Cerutti, J. Guardia-Valenzuela, J. Molson
CERN, Geneva, Switzerland

Abstract

The target peak luminosity of the CERN FCC-hh during Pb-Pb collisions is more than a factor of 50 greater than that achieved by the LHC in 2018. As a result, the intensity of secondary beams produced in collisions at the interaction points will be significantly higher than previously experienced. With up to 72 kW deposited in a localised region by a single secondary beam type, namely the one originated by Bound Free Pair Production (BFPP), it is essential to develop strategies to safely intercept these beams, and also the ones from ElectroMagnetic Dissociation (EMD), in order to ensure successful FCC-hh Pb-Pb operation. A series of beam tracking and energy deposition simulations were performed to determine the optimal solution for handling the impact of such beams. In this contribution the most advanced results are presented, with a discussion of different options.

INTRODUCTION

The Future Circular Collider (FCC) study [1] provides a description of a novel research infrastructure aimed at extending the energy frontier by almost an order of magnitude. A new highest-energy hadron collider, FCC-hh, will provide proton-proton collisions at a centre of mass energy of 100 TeV, with additional foreseen heavy-ion operation involving ion-proton and ion-ion collisions [2].

One of the major challenges associated with such high-energy heavy-ion collisions arises from ultra-peripheral electromagnetic interactions of the interacting beams, which lead to secondary beams. Since these beams do not have the reference magnetic-rigidity, they will follow a dispersive orbit trajectory, and eventually impact the physical beam pipe aperture, delivering steady-state power in unwanted locations [3–7]. In order to avoid quenching the impacted superconducting magnets, the beams must be absorbed by robust collimators on either side of the interaction points (IPs), or diverted by an orbit bump into a non-critical loss location, as in LHC and soon HL-LHC [7, 8].

The two processes responsible for the highest powered secondary beams are Bound Free Pair Production (BFPP) and Electromagnetic Disassociation (EMD). In BFPP interactions, an outgoing ion captures an electron from an e^+e^- pair, leading to a change in its effective charge and thus rigidity: ${}^{A}X^{Z+} + {}^{A}X^{Z+} \rightarrow {}^{A}X^{Z+} + {}^{A}X^{(Z-1)+} + e^+$. EMD interactions conversely produce an excited ion nucleus emitting one or more nucleons, with the most common process being neutron emission, and leaving the IP with a reduced total momentum: ${}^{A}X^{Z+} + {}^{A}X^{Z+} \rightarrow {}^{A}X^{Z+} + {}^{(A-1)}X^{Z+} + n$. The highest cross section EMD channels are EMD1, with the emission of one neutron, and EMD2, with two neutrons. The power carried by these secondary beams is computed as $P = \sigma L E_s$, where σ is the respective interaction cross sections, L the luminosity and E_s is the secondary beam particle energy.

A comparison of the quantities used to calculate the power of the secondary beams in LHC and FCC during lead-lead collisions can be found in Table 1. It is clear that the FCC's significant improvement in luminosity is largely responsible for the orders-of-magnitude increase in the power of all secondary beams, whilst the higher energy of the primary beams also plays a significant role.

Table 1: Relevant Quantities for Secondary Beams Generated in Lead-Lead Collisions, Comparison Between LHC and FCC [1]. Cross Sections Correspond to a Single Side, With Values for σ_{EMD} Obtained With FLUKA [9–12]

Quantity	LHC	FCC
L (10^{27} cm^{-2}s^{-1})	6	320
σ_{BFPP} (10^{-27} cm^2)	280	344
σ_{EMD1} (10^{-27} cm^2)	95	119
σ_{EMD2} (10^{-27} cm^2)	30	37
E (Z TeV)	7	50
P, BFPP (kW)	0.15	72
P, EMD1 (kW)	0.055	25
P, EMD2 Power (kW)	<0.02	8

TRACKING OF SECONDARY BEAMS

The optical configuration used for the study was the FCC-hh lattice as of summer 2020 [1]. Since no dedicated Pb ion optics currently exists, the standard proton optics were used in the collision configuration. Here the reference energy, E, is 50 Z TeV, which for Pb ions gives a total energy of 4100 TeV. The crossing angle was set to 100 µrad, and the β-function at the IP was squeezed to 30 cm.

Sixtrack V5.4.3 [13] was used to track particles in the secondary beams. Bunches matched into the accelerator lattice were generated at the interaction point "IPA" for beam 1 and were tracked until the dispersion suppressor.

It was decided to track the 3 secondary beam species with the highest power load, i.e. ${}^{208}_{82}\mathrm{Pb}^{81+}$ from BFPP1, ${}^{207}_{82}\mathrm{Pb}^{82+}$ from EMD1, and ${}^{206}_{82}\mathrm{Pb}^{82+}$ from EMD2. Other secondary beams with lower reaction cross sections will contribute a much lower power load, and they are ignored for this study.

For the BFPP beam, the ions were kept at the reference beam energy, but had their charge changed from 82+ to 81+. For the EMD beams, the rest mass was reduced (depending

* james.hunt@cern.ch

Content from this work may be used under the terms of the CC BY 3.0 licence (© 2021). Any distribution of this work must maintain attribution to the author(s), title of the work, publisher, and DOI

ISBN: 978-3-95450-214-1 ISSN: 2673-5490 doi:10.18429/JACoW-IPAC2021-WEPAB025

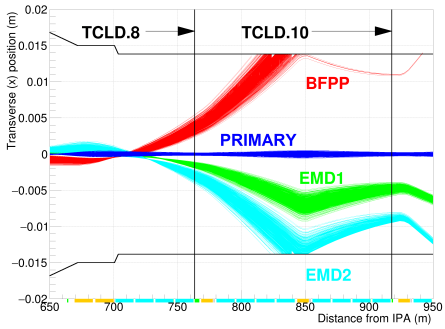

Figure 1: Secondary beam trajectories coming from the IP with the s positions of TCLD.8 and TCLD.10 marked by two vertical lines.

on the number of lost nucleons) and the total ion energies were also reduced correspondingly. These beams were then tracked (as seen in Fig. 1) and their full phase space coordinates were dumped at an assortment of locations for loading into FLUKA.

Initial attempts to stop the secondary beams in the matching section (where there is plenty of available space to insert additional collimators as absorbers) were not successful due to the lack of sufficient dispersion in this region, and therefore a lack of separation of the secondary beams from the core circulating beam. It was therefore chosen to attempt to stop all secondary beams inside the dispersion suppressor, where the dispersion is higher and space exists for installing collimators. Initially, two collimators are present in the lattice, called TCLD.8 (in cell 8) and TCLD.10 (in cell 10).

Figure 2 shows the transverse distributions of the beams at the entrance of TCLD.8 and two potential schemes for collimation at this location. In "Scheme 1" the goal is to safely remove EMD2 and BFPP1 using TCLD.8, allowing EMD1 to continue to TCLD.10 where it may be independently captured. "Scheme 2" attempts to capture the three beams on TCLD.8 alone.

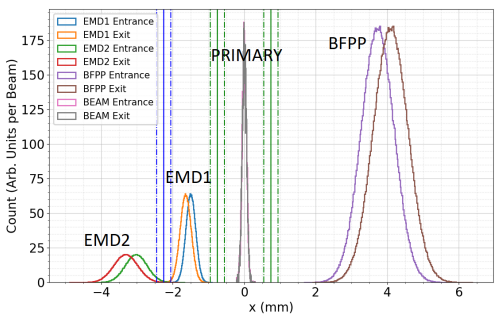

Figure 2: Transverse beam distributions at the entrance and exit of TCLD.8. Secondary beam distributions have been scaled in proportion to their relative power, the primary distribution is not. Scheme 2 (green) jaw positions are indicated between 200 µm error tolerance estimates as solid and dashed vertical lines respectively, with negative x jaw position for Scheme 1 in blue.

COLLIMATOR DESIGN AND ENERGY DEPOSITION SIMULATIONS

In order to test the collimation schemes, energy deposition simulations in FLUKA were performed. Using the Python-based program Line Builder [14], it is possible to simulate large and complex 3D geometries of beamlines in FLUKA. About 200 m of the dispersion suppressor were constructed, from cell 8 to cell 10 inclusive, consisting of 12 × 14.3 m superconducting dipoles, and 3 × 9.2 m superconducting quadrupoles. To model TCLD.8, upstream from the first quadrupole in cell 9, an elongated version of the LHC's TCT collimator geometry was used, split into several modules. This 3D model includes the copper housing around the active material, tapered jaws and cooling pipes. Since the beams to be intercepted by this collimator carry such high power, the active material of the jaws was extended outwards horizontally from 2 cm thickness to 3 cm thickness per jaw.

For each of the considered secondary beams, distributions generated in SixTrack 10 cm upstream of the collimator entrance were used as initial conditions in FLUKA. The energy deposition on the collimator jaws and in the coils of the downstream magnets was recorded in a fine mesh. Design limits on the peak power density in the collimator jaws of 1 kW/cm^3, as well as a quench limit of 70 mW/cm^3 in the downstream magnetic coils were assumed.

Several materials were considered for the active parts of the jaws, including two types of novel graphite-based composites (reinforced with molybdenum) [15], MoGRGM64 (ρ = 2.48 g/cm^3) and MoGRFCC1 (ρ = 3.81 g/cm^3). Additionally, a copper diamond alloy (CuDI ρ = 5.42 g/cm^3) and a high density tungsten-based alloy, Inermet [16], were included in the list of explored materials. A maximum load of 1 kW per metre of length was accepted for Inermet, with CuDI up to 3 kW per m in length, and the molybdenum-graphite based composites up to 15 kW per m in length.

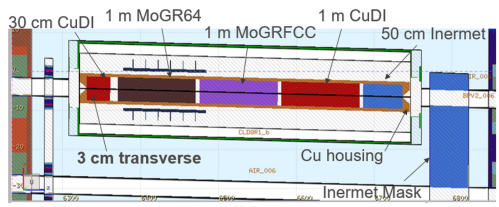

Figure 3: Longitudianl layout of collimator jaws shown in Flair [17] (beam direction left to right).

With these restrictions, iterative simulations were used to determine an optimised configuration for the material choice and block lengths in the collimators. Since it carries the highest power, the BFPP beam was used during this process. The obtained design is shown in Fig. 3. The block lengths were restricted to 1 m, 50 cm and 30 cm for ease of analysis in thermal load simulations but may be further optimised. The longitudinal sequence of materials has been selected such that a shower may be first induced by the medium-density yet robust CuDI. During the full development of the shower,

Content from this work may be used under the terms of the CC BY 3.0 licence (© 2021). Any distribution of this work must maintain attribution to the author(s), title of the work, publisher, and DOI

ISBN: 978-3-95450-214-1 ISSN: 2673-5490 doi:10.18429/JACoW-IPAC2021-WEPAB025

Content from this work may be used under the terms of the CC BY 3.0 licence (© 2021). Any distribution of this work must maintain attribution to the author(s), title of the work, publisher, and DOI

when it reaches its maximum intensity, two longer blocks of low-density, highly robust MoGR are employed to prevent overheating. These blocks are placed in order of increasing density, with CuDI and Inermet blocks following soon after to robustly absorb the now diluted shower. Careful attention was paid to configure the lengths to exploit the robustness of lower-density low-Z materials, whilst balancing shower containment and maximum load allowed on the high absorption rates of higher-density high-Z materials. To reduce the amount of energy arriving at the front face of the downstream quadrupole in the vertical plane, an Inermet mask was placed between the collimator and quadrupole.

With the collimator design optimised, the Scheme 1 and Scheme 2 were investigated. In Scheme 1, where the two slightly overlapping EMD beams are split, the EMD2 beam was simulated first. Because of a small but non-negligible fraction of the impacts along the face of the jaw, and due to shallow penetration into the tapering causing secondary shower particles to escape the collimator, a disproportionately large peak power density was seen in the downstream coils. For this reason, it was determined that an extreme sensitivity to the jaw positioning and orbit of the secondary beams does not guarantee a safe value for peak power density in the downstream coils using this collimation scheme, which is therefore not studied further.

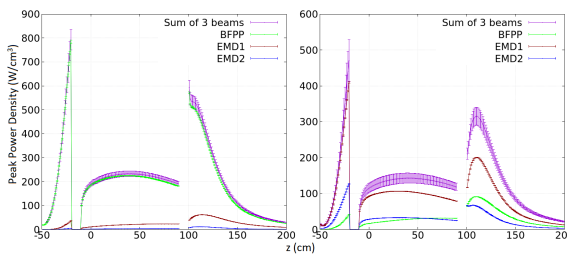

Figure 4: Peak power density profiles on the first 3 blocks of the outer (left) and inner (right) jaws of TCLD.8 due to all three secondary beams.

For Scheme 2, where TCLD.8 removes all three secondary beams, the EMD1 beam was considered first. The maximum peak power density observed in the downstream coils was 22 mW/cm^3, which is well below the quench limit. A lower value of 19 mW/cm^3 was observed for the BFPP beam, due to a deeper impact into the tapering. For the EMD2 beam the signal on the downstream coils was negligible.

The sum of the contributions from all three beams on the jaws may be seen in Fig. 4. For the positive jaw, the contribution is dominated by the BFPP, as expected. The third blocks on both jaws, containing MoGRFCC1, receive the highest loads at 13.6 kW and 9.4 kW for the positive and negative x jaws, respectively. For this reason the energy deposition maps for these were analysed to determine the thermo-mechanical behaviour during operation.

THERMAL LOAD SIMULATIONS

The energy deposition map from FLUKA, including the contributions from the three beams, was used as input in a steady-state thermal Finite Element Modelling (FEM) simulation. The resulting temperature map served as input for a static-structural FEM simulation, calculating the deformation of the jaws. Both numerical analyses were performed with ANSYS® code [18]. The MoGRFCC1 material was oriented for optimum thermal transfer to the cooling system, therefore minimising the maximum temperature (T_{max}).

The total power deposited on the most loaded jaw is 22.0 kW (13.6 kW on the absorber blocks), resulting in T_{max} of 204 °C and maximum dynamic deformation (δ_{max}) of 1 060 µm towards the beam. The opposite jaw receives a total power of 17 kW (9.4 kW on the blocks), resulting in T_{max} of 136 °C and δ_{max} of 800 µm also towards the beam.

Several possible design changes were studied to reduce those jaw deformations, which are unacceptable given that the needed collimator half gap is around 750–900 µm. The jaw stiffener structure and the housing of the absorber blocks are made of a copper alloy (GLIDCOP® AL-15 [19]) in current collimators. Changing the housing material to Mo was found to reduce the deformation. Despite Mo having lower thermal conductivity than Cu (resulting in slightly higher T_{max}), its lower coefficient of thermal expansion leads to less δ_{max}. Another possible option is to split the jaw in several independently-supported parts. The numerical results with different jaw designs are summarised in Table 2.

Table 2: Simulation Results With Different Jaw Designs

Jaw	L	R	L	R	L	R
Housing	Cu	Cu	Mo	Mo	Mo	Mo
Sections	1	1	1	1	4	4
T_{max} (°C)	204	136	291	181	296	188
δ_{max} (μm)	1060	800	530	380	**150**	**90**

CONCLUSIONS

The secondary beams generated during Pb ion operation at the FCC-hh carry a total power of more than 100 kW that is continuously lost in the dispersion suppressor. Safely disposing of this power, continuously impacting on collimators during collisions, poses an extreme challenge in the collider design. We have investigated different collimator layouts and designs through iterative simulations with SixTrack, FLUKA and ANSYS®. An optimised preliminary layout has been established, accounting for the load on downstream coils and the collimators. We expect no permanent damage on the collimators, but very challenging dynamic deformations are simulated, which might be mitigated by splitting the collimators in many smaller modules. This work shows that a solution may be within reach, in spite of the very high beam loss power, although further work is still needed to further improve and optimise the collimator design. Outgassing due to the high temperatures should also be investigated.

ACKNOWLEDGEMENTS

We are very grateful to M. Schaumann and J. M. Jowett for useful discussions and early inputs to these studies.

ISBN: 978-3-95450-214-1 ISSN: 2673-5490 doi:10.18429/JACoW-IPAC2021-WEPAB025

REFERENCES

[1] A. Abada *et al.*, "FCC-hh: The Hadron Collider", CERN, Geneva, Switzerland, Rep. CERN-ACC-2018-0058, Dec. 2018.

[2] M. Schaumann, "Potential performance for Pb-Pb, *p*-Pb, and *p*–*p* collisions in a future circular collider", *Phys. Rev. ST Accel. Beams*, vol. 18, p. 091002, Sep. 2015. doi:10.1103/PhysRevSTAB.18.091002

[3] S. R. Klein, "Localized beampipe heating due to e- capture and nuclear excitation in heavy ion colliders", *Nucl. Inst. & Methods A*, vol. 459, p. 51, 2001. doi:10.1016/S0168-9002(00)00995-5

[4] R. Bruce *et al.*, "Observations of beam losses due to bound-free pair production in a heavy-ion collider", *Phys. Rev. Letters*, vol. 99, no. 14, p. 144801, 2007. doi:10.1103/PhysRevLett.99.144801

[5] R. Bruce *et al.*, "Beam losses from ultraperipheral nuclear collisions between Pb ions in the Large Hadron Collider and their alleviation", *Phys. Rev. ST Accel. Beams*, vol. 12, p. 071002, Jul 2009. doi:10.1103/PhysRevSTAB.12.071002

[6] J. M. Jowett and M. Schaumann, "FCC-hh as a heavy-ion collider", presented at FCC week, Washington DC., USA, Mar. 2015, unpublished. https://indico.cern.ch/event/340703/contributions/802113/

[7] M. Schaumann *et al.*, "Bound-free pair production from nuclear collisions and the steady-state quench limit of the main dipole magnets of the CERN Large Hadron Collider", *Phys. Rev. Accel. Beams*, vol. 23, no. 12, p. 121003, Dec. 2020. doi:10.1103/PhysRevAccelBeams.23.121003

[8] S. Redaelli *et al.*, "Chapter 5: Collimation system," in *High-Luminosity Large Hadron Collider (HL-LHC): Technical design report vol. 10*, I. Béjar Alonso, O. Brüning, P. Fessia, L. Rossi, L. Tavian, M. Zerlauth Eds., Geneva, Switzerland: CERN Yellow Rep. Monogr., 2020, pp. 87–114.

[9] FLUKA, http://fluka.cern

[10] G. Battistoni *et al.*, "Overview of the FLUKA code", *Annals of Nuclear Energy*, vol. 82, pp. 10-18, 2015. doi:10.1016/j.anucene.2014.11.007

[11] T. T. Bohlen *et al.*, "The FLUKA Code: Developments and Challenges for High Energy and Medical Applications", *Nuclear Data Sheets*, vol. 120, pp. 211-214, 2014. doi:10.1016/j.nds.2014.07.049

[12] S. Roesler, R. Engel, and J. Ranft, "The Monte Carlo Event Generator DPMJET-III", in *Advanced Monte Carlo for Radiation Physics, Particle Transport Simulation and Applications*, A. Kling, F. J. C. Barão, M. Nakagawa, L. Távora, P. Vaz Eds. Berlin, Heidelberg, Germany: Springer, 2001, pp. 1033–1038. doi:10.1007/978-3-642-18211-2_166

[13] R. De Maria *et al.*, "SixTrack Version 5: Status and New Developments", in *Proc. 10th Int. Particle Accelerator Conf. (IPAC'19)*, Melbourne, Australia, May 2019, pp. 3200–3203. doi:10.18429/JACoW-IPAC2019-WEPTS043

[14] A. Mereghetti, V. Boccone, F. Cerutti, R. Versaci, and V. Vlachoudis, "The FLUKA LineBuilder and Element DataBase: Tools for Building Complex Models of Accelerator Beam Lines", in *Proc. 3rd Int. Particle Accelerator Conf. (IPAC'12)*, New Orleans, LA, USA, May 2012, paper WEPPD071, pp. 2687–2689.

[15] J. Guardia-Valenzuela, "Development and properties of high thermal conductivity molybdenum carbide - graphite composites", *Carbon*, vol. 135, pp. 72-84, Aug 2018. doi:10.1016/j.carbon.2018.04.010

[16] PLANSEE - Tungsten heavy alloys, https://www.plansee.com/en/materials/tungsten-heavy-metal.html

[17] V. Vlachoudis, "FLAIR: A Powerful But User Friendly Graphical Interface For FLUKA", in *Proc. Int. Conf. on Mathematics, Computational Methods & Reactor Physics (M&C 2009)*, Saratoga Springs, New York, 2009, paper 2749540, pp. 790-800. http://cds.cern.ch/record/2749540

[18] ANSYS Inc., 'Ansys Mechanical User's Manual - Release 2019 R1.

[19] Hoganas - GLIDCOP, https://www.hoganas.com/en/powder-technologies/glidcop/

Content from this work may be used under the terms of the CC BY 3.0 licence (© 2021). Any distribution of this work must maintain attribution to the author(s), title of the work, publisher, and DOI